CFD Modeling and Simulation of the riser of an Industrial Residue Fluid Catalytic Cracking (RFCC) unit

Aisha Ahmed, A. Maulud, M. Ramasamy, K.K. Lau, and S. Mahadzir

Chemical Engineering Department, Universiti Teknologi PETRONAS
31750, Tronoh, MALAYSIA

***Abstract- A* 2D axi-symmetric, steady state and pressure-based model for the riser of an industrial RFCC unit was developed with ANSYS FLUENT in workbench 13.0. The Eulerian–Eulerian approach was applied to simulate the flow behavior of the two phases and the catalytic cracking reactions. The k-ε gas–solid turbulent flow per phase model was used, and the particle-level fluctuations are modeled in the framework of the kinetic theory of granular flow. Two different drag models were used separately to simulate the gas solid interaction in the riser fluidized bed. The 14-lump kinetic model was chosen to describe the complex catalytic cracking of the heavy residual feed stock. The particle volume fraction, velocity and temperature profiles, as well as product yields in the riser were analyzed and validated with results from open literature and plant data.**

I. INTRODUCTION

Fluid catalytic cracking process (FCC) is one of the most extensively used operations for the conversion of gas oil and certain atmospheric residues to upgraded gasoline and lighter products. It is sometimes referred to as the heart of the refinery. Therefore, several studies have been conducted for FCC modeling, simulation, optimization and control, but very few of them consider the residual feed stocks in residue fluid catalytic cracking (RFCC) unit. The features of RFCC technology, such as the special feed injection system, the mix temperature control (MTC), riser termination device, and the Amoco product vapor quench, help to improve the product selectivity, unit capacity, and operability of the unit [1]. Most of these features are in the feed-catalyst contacting zone. In the riser of the RFCC, lift steam suspends the catalyst particles extending its bed upward to the feed injection point. The feed enters as liquid droplets along with atomizing steam, contacts the hot catalyst, and rapidly evaporates. As the suspension of catalyst powder in reactant gases rises upward, the gas is cracked to lighter hydrocarbons (gasoline and light gases) and coke. The product vapor and gases are separated from the catalyst particles immediately after the riser end by special disengager and cyclones to terminate any further reactions.

Extensive works had been done on the heat-transfer in the liquid/gas/solids systems in the feed-catalyst contacting zone [2-5]. The time required to vaporize droplets is directly related to their size, therefore small droplets size with uniform distribution are desired in the riser feed atomizer [2]. Theologos *et al*., [2] assumed that reaction only occurred above the riser height corresponding to a complete vaporization. Berry *et al*., [3] considered simultaneous reaction and vaporization effects. They derived physical equations relating the heating up time and vaporization time to the droplet diameter, using void fraction and slip velocity from their hydrodynamic model. On the other hand many studies [6-8] developed two phase model (gas-solid phase) for the riser of FCC unit assuming instantaneous feed vaporization *i.e.,* 100% vaporization occurs right at the moment of contact with the hot regenerated catalyst.

It is realized that the mathematical complexity due to the nonlinearity of the equations defining the interpenetrating and moving phase boundaries in multiphase systems with stiff kinetic model equations make numerical solutions very difficult. With the development of high performance computers and advances in numerical techniques and algorithms, computational fluid dynamics (CFD) tools are increasingly gaining popularity. FLUENT is a state-of-the-art computer program for modeling fluid flow and heat transfer in complex geometries. It provides complete mesh flexibility, solving any flow problem with unstructured meshes that can be generated about complex geometries in 2D or 3D with relative ease. Therefore, many research studies have been employing the CFD modeling for the FCC riser and downer reactors [8-12]. In the last decade, CFD technique has received much more attention when modeling a gas-solid multiphase flow reactor. In this type of reactors, the discrete particle phase can be treated as a pseudo continuous fluid (Eulerian–Eulerian scheme) or a discrete element (Eulerian–Lagrangian scheme). The advantage of the Eulerian–Eulerian scheme is the consistent form of governing equations, which allows for efficient computation of practical engineering problems. However, since the particle-scale information is not included in such models, a chemically reacting flow that is sensitive to the instantaneous particle properties such as the catalyst activity versus time cannot be reasonably described by the Eulerian–Eulerian models from a theoretical point of view. Although the Eulerian-Lagrangian approach is very promising, it is very computationally expensive. Although it is possible to follow all the particles in modestly sized devices only at extremely low particle volume fractions, it is currently not possible to simulate large number of particles encountered in large-scale fluidized beds. The Eulerian multiphase model allows for the modeling of multiple, separate, yet interacting phases that the Eulerian treatment is used for each phase, in contrast to the Eulerian – Lagrangian treatment which is used for the discrete phase model. The differences between the above two modeling strategies, were evaluated by Hernandez-Jimenez *et al*., [9]. They found that for a given coefficient of friction, both simulation strategies yield time-averaged velocities with

similar magnitudes, and different velocity profiles. The two-fluid model predicts that the highest velocities within the bed are located at a distance near wall, whereas the Discrete Element Model (DEM) predicts that the highest velocities are located at the centre of the bed. For both simulation techniques, the time-averaged solids volume fractions show minima that coincide with the maxima in the velocity profiles [9].

The advantages of modeling the cracking kinetics with more than 10 lumps are: (i) a single group of estimated kinetic constants can be used for various feedstocks; and (ii) all the most important FCC products can be predicted separately. However, large number of kinetic constants must be estimated, that may increase the complexity of the numerical solution exponentially [6]. The cracking reaction was simulated with a simple three-lump kinetic model by Theologos and Markatos [10] and compared with a detailed 10-lump reaction kinetics scheme and feed spray vaporization effect of Theologos *et al*., [2]. But in the above two works, turbulent flow and the diffusion of particle phase was not considered. On the other hand, the particle-level fluctuations are modeled in the framework of the kinetic theory of granular flow, together with a 12- lump kinetic model by Das *et al.*, [8], to study the effect of the flow on the reaction variables.

The k-ε-k_p-ε_p-Θ gas–solid turbulent flow, based on the kinetic theory of granular flow simulates both the gas phase and particle phase by low Reynolds number turbulent model [11, 12]. The turbulence of particles was considered similar to the motion of eddies in single-phase turbulent flow. In fact, there exist appreciable differences between the particle collisions and particles turbulence. This model together with the 14-lump kinetics model was used to analyze the distributions of particle volume fraction and velocity, as well as product yields in the two-stage riser fluid catalytic cracking (TSRFCC) reactors [12].

A comparison between different drag models [13-15] was made by Almuttahar and Taghipour [16] and found that the predictions of the solid volume fraction and axial particle velocity are similar. However, the drag model modified based on the minimum fluidization condition [15] showed a better solid volume fraction prediction at the core area [16].

Figure 1 shows all types of force interactions in gas –solid flow systems [17]. A systematic analysis of various interactions in the downer, via, gas phase interactions (turbulence), particle phase interactions (particle–particle collisions) and interphase interactions (drag) was performed [17]. The interaction between fluctuating fields of gas phase and solids phase was not taken into account, as it is expected

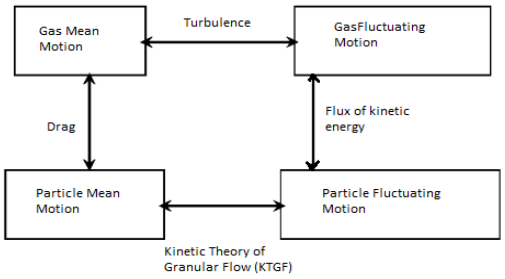

Figure 1. Types of interactions in gas–solid dispersed flow.[17]

to be a correlation of lower order compared to other three interactions. According to the investigations, carried by Vaishali *et al.*, [17] for the most suitable closures of force interactions in the gas-solid flow system, it was found that the drag closure developed by Matsen [18], with a suitably modified exponent depending upon the operating conditions, is able to predict the average flow well and also predicts higher slip velocity as compared to other investigated drag closures.

All the various drag models that was examined and compared by Peng *et al.*, [19] failed to describe the turbulence in the riser either due to underestimation or overestimation of the drag force between the gas and the solid phase. To account for the fact that the drag force is affected by the degree of clustering and which in turn is affected by the void fraction, they proposed a four-zone drag model to calculate the gas–solid exchange coefficient in the turbulent fluidization of FCC particles [19].

All the above works and those in literature are simulating the riser or downer of FCC unit with its gas oil feedstock. In this work an industrial RFCC riser with high Conradson carbon residue feedstock is modeled and simulated using CFD tools. An instantaneous feed vaporization is assumed, correcting the feed and catalyst temperatures by making heat balance equation at the point of contact. The two dimensional steady-state model equations for the riser are to be solved using FLUENT in ANSYS Workbench 13.0. Solids are modeled as pseudo-fluid using kinetic theory of granular flow, and the modified Matsen's drag model [17] is used. Also for the turbulence model, the standard k-ε per phase viscous model is chosen depending on several considerations such as the physics encompassed in the flow, the level of accuracy required, the available computational resources, and the amount of time available for the simulation. The 14-lump kinetic model is combined with the 2D component continuity equation. The results are compared with an industrial plant data, and other works in open literature.

II. RFCC Riser Model

For the gas-solid upward flow system in the riser sketched in Figure 2, the developed steady-state mass, momentum and energy conservation equations for each phase are:

A. *Gas phase:*

Continuity

$$\frac{\partial}{\partial r}(r\varepsilon_g\rho_g v_r)+\frac{\partial}{\partial z}(\varepsilon_g\rho_g v_z)=0 \qquad (1)$$

Component continuity

$$\frac{\partial}{\partial z}(\varepsilon_g\rho_g C_i v_z)+\frac{1}{r}\frac{\partial}{\partial r}(r\varepsilon_g\rho_g C_i v_r)= \frac{\partial}{\partial z}\left(D_m\varepsilon_g\rho_g\frac{\partial}{\partial z}C_i\right)+\frac{1}{r}\frac{\partial}{\partial r}\left(rD_m\varepsilon_g\rho_g\frac{\partial}{\partial r}C_i\right)+r_i \qquad (2-15)$$

Momentum

$$\frac{\partial}{\partial r}(\varepsilon_g\rho_g v_r v_r)+\frac{\partial}{\partial z}(\varepsilon_g\rho_g v_r v_z)= -\frac{\partial(P+\frac{2}{3}\rho_g k)}{\partial r}-\left[\frac{1}{r}\frac{\partial}{\partial r}(r\varepsilon_g\tau_{rrr})+\frac{\partial}{\partial z}(\varepsilon_g\tau_{rrz})\right] +\varepsilon_g\rho_g g_r-\beta(v_r-V_{pr}) \qquad (16)$$

$$\frac{\partial}{\partial r}(\varepsilon_g\rho_g v_z v_r)+\frac{\partial}{\partial z}(\varepsilon_g\rho_g v_z v_z)= -\frac{\partial P}{\partial z}-\left[\frac{1}{r}\frac{\partial}{\partial r}(r\varepsilon_g\tau_{zrr})+\frac{\partial}{\partial z}(\varepsilon_g\tau_{zrz})\right]+\varepsilon_g\rho_g g_z -\beta(v_z-V_{pz}) \qquad (17)$$

where viscous gas phase stresses are:

$$\tau_{grr} = -\left[\left(\xi_g - \frac{2}{3}\mu_g\right)\left(\frac{\partial v_r}{\partial r}\right) + (\mu_g + \mu_g^t)\left[\frac{1}{r}\frac{\partial (r v_r)}{\partial r} + \frac{\partial v_z}{\partial z} + \frac{\partial v_r}{\partial z} + \frac{1}{r}\frac{\partial (r v_z)}{\partial r}\right]\right]$$

$$\tau_{grz} = -\left[\left(\xi_g - \frac{2}{3}\mu_g\right)\left(\frac{\partial v_r}{\partial z}\right) + (\mu_g + \mu_g^t)\left[\frac{1}{r}\frac{\partial (r v_r)}{\partial r} + \frac{\partial v_z}{\partial z} + \frac{\partial v_r}{\partial z} + \frac{1}{r}\frac{\partial (r v_z)}{\partial r}\right]\right]$$

$$\tau_{gzr} = -\left[\left(\xi_g - \frac{2}{3}\mu_g\right)\left(\frac{\partial v_z}{\partial r}\right) + (\mu_g + \mu_g^t)\left[\frac{1}{r}\frac{\partial (r v_r)}{\partial r} + \frac{\partial v_z}{\partial z} + \frac{\partial v_r}{\partial z} + \frac{1}{r}\frac{\partial (r v_z)}{\partial r}\right]\right]$$

$$\tau_{gzz} = -\left[\left(\xi_g - \frac{2}{3}\mu_g\right)\left(\frac{\partial v_z}{\partial z}\right) + (\mu_g + \mu_g^t)\left[\frac{1}{r}\frac{\partial (r v_r)}{\partial r} + \frac{\partial v_z}{\partial z} + \frac{\partial v_r}{\partial z} + \frac{1}{r}\frac{\partial (r v_z)}{\partial r}\right]\right]$$

Energy

$$\frac{\partial}{\partial r}(\varepsilon_g \rho_g H_g v_r) + \frac{\partial}{\partial z}(\varepsilon_g \rho_g H_g v_z) = \frac{1}{r}\frac{\partial}{\partial r}\left[r\varepsilon_g(\lambda + \lambda^t)\frac{\partial T}{\partial r}\right] + \frac{\partial^2}{\partial z^2}\left[\varepsilon_g(\lambda + \lambda^t)T\right] - \frac{1}{r}\frac{\partial}{\partial r}\left(r\left(P + \frac{2}{3}\rho_g k\right)v_r\right) - \frac{\partial}{\partial z}\left(\left(P + \frac{2}{3}\rho_g k\right)v_z\right) - \left\{\frac{\partial}{\partial r}(\varepsilon_g \tau_{grr} v_r) + \frac{\partial}{\partial z}(\varepsilon_g \tau_{grz} v_z) + \frac{\partial}{\partial r}(\varepsilon_g \tau_{gzr} v_z) + \frac{\partial}{\partial z}(\varepsilon_g \tau_{gzz} v_r)\right\} - \frac{\beta}{2}\left[(v_r, v_r - V_{gr}, V_{gr}) + (v_z, v_z - V_{gz}, V_{gz})\right] + h_{fg} a_s (T_s - T) + \varepsilon_g \rho_g (g_r v_r + g_z v_z) - \beta\left(k - \frac{3}{2}\theta\right) \quad (18)$$

B. Solid phase:

It is expected that the momentum and energy transfer will be different according to the granular regimes. In kinetic theory of granular flow, the granular temperature ($\theta = \frac{1}{3}\langle c^2\rangle$ in m^2/s^2) describes the particle–particle collisions and is a measure of the random fluctuation of single particle, where the fluctuating energy per unit mass is ($E_\theta = \frac{1}{2}\langle c^2\rangle = \frac{3}{2}\theta$). In fact, granular temperature describes the particle motions in micro scale. But in fluidized beds, including risers, there exist particle motions in the larger scale, for example, the random motion of clusters.

Continuity equation

$$\frac{1}{r}\frac{\partial}{\partial r}(r\varepsilon_s \rho_{ss} V_{gr}) + \frac{\partial}{\partial z}(\varepsilon_s \rho_{ss} V_{gz}) = 0 \quad (19)$$

Momentum

$$\frac{\partial}{\partial r}(\varepsilon_s \rho_{ss} V_{gr}, V_{gr}) + \frac{\partial}{\partial z}(\varepsilon_s \rho_{ss} V_{gr}, V_{gz}) = -\frac{\partial P_s}{\partial r} - \left[\frac{1}{r}\frac{\partial}{\partial r}(r\varepsilon_s \tau_{srr}) + \frac{\partial}{\partial z}(\varepsilon_s \tau_{srz})\right] + \varepsilon_s \rho_{ss} g_r + \beta(v_r - V_{gr}) \quad (20)$$

$$\frac{\partial}{\partial r}(\varepsilon_s \rho_{ss} V_{gz}, V_{gr}) + \frac{\partial}{\partial z}(\varepsilon_s \rho_{ss} V_{gz}, V_{gz}) = -\frac{\partial P_s}{\partial z} - \left[\frac{1}{r}\frac{\partial}{\partial r}(r\varepsilon_s \tau_{szr}) + \frac{\partial}{\partial z}(\varepsilon_s \tau_{szz})\right] + \varepsilon_s \rho_{ss} g_z + \beta(v_z - V_{gz}) \quad (21)$$

where the solid phase stresses are:

$$\tau_{srr} = -\left[\left(\xi_s - \frac{2}{3}\mu_s\right)\left(\frac{\partial V_{gr}}{\partial r}\right) + \mu_s\left[\frac{1}{r}\frac{\partial (r V_{gr})}{\partial r} + \frac{\partial V_{gz}}{\partial z} + \frac{\partial V_{gr}}{\partial z} + \frac{1}{r}\frac{\partial (r V_{gz})}{\partial r}\right]\right]$$

$$\tau_{srz} = -\left[\left(\xi_s - \frac{2}{3}\mu_s\right)\left(\frac{\partial V_{gr}}{\partial z}\right) + \mu_s\left[\frac{1}{r}\frac{\partial (r V_{gr})}{\partial r} + \frac{\partial V_{gz}}{\partial z} + \frac{\partial V_{gr}}{\partial z} + \frac{1}{r}\frac{\partial (r V_{gz})}{\partial r}\right]\right]$$

$$\tau_{szr} = -\left[\left(\xi_s - \frac{2}{3}\mu_s\right)\left(\frac{\partial V_{gz}}{\partial r}\right) + \mu_s\left[\frac{1}{r}\frac{\partial (r V_{gr})}{\partial r} + \frac{\partial V_{gz}}{\partial z} + \frac{\partial V_{gr}}{\partial z} + \frac{1}{r}\frac{\partial (r V_{gz})}{\partial r}\right]\right]$$

$$\tau_{szz} = -\left[\left(\xi_s - \frac{2}{3}\mu_s\right)\left(\frac{\partial V_{gz}}{\partial z}\right) + \mu_s\left[\frac{1}{r}\frac{\partial (r V_{gr})}{\partial r} + \frac{\partial V_{gz}}{\partial z} + \frac{\partial V_{gr}}{\partial z} + \frac{1}{r}\frac{\partial (r V_{gz})}{\partial r}\right]\right]$$

Granular temperature

Conservation of the granular temperature or the granular fluctuating energy yields:

$$\frac{3}{2}\left[\frac{1}{r}\frac{\partial}{\partial r}(r\varepsilon_s \rho_{ss}\theta V_{gr}) + \frac{\partial}{\partial z}(\varepsilon_s \rho_{ss}\theta V_{gz})\right] = \frac{1}{r}\frac{\partial}{\partial r}(r P_s V_{gr}) - \frac{\partial}{\partial z}(P_s V_{gz}) - \varepsilon_s\left[\tau_{srr}\frac{\partial}{\partial r}V_{gr} + \tau_{srz}\frac{\partial}{\partial z}V_{gr} + \tau_{szr}\frac{\partial}{\partial r}V_{gz} + \tau_{szz}\frac{\partial}{\partial z}V_{gz}\right] - \frac{\partial}{\partial r}(\varepsilon_s q_r) - \frac{\partial}{\partial z}(\varepsilon_s q_z) - 3\beta\theta - \gamma \quad (22)$$

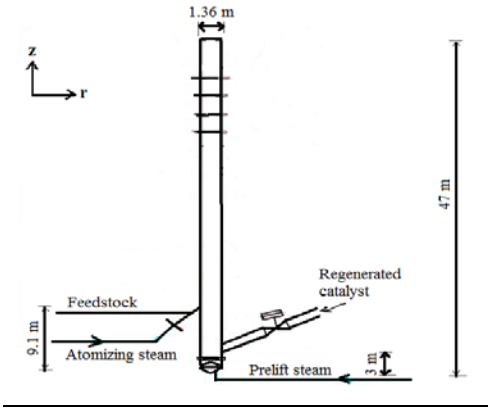

Figure 2. Riser geometry

C. Turbulent kinetic energy (in both phases):

$$\frac{\partial}{\partial r}(\varepsilon_g \rho_g k v_r) + \frac{\partial}{\partial z}(\varepsilon_g \rho_g k v_z) = \frac{1}{r}\frac{\partial}{\partial r}\left[r\varepsilon_g\left(\frac{\mu_g + \mu_g^t}{\sigma_k}\right)\frac{\partial k}{\partial r}\right] + \frac{\partial^2}{\partial z^2}\left[\varepsilon_g\left(\frac{\mu_g + \mu_g^t}{\sigma_k}\right)k\right] + \left[\varepsilon_g \mu_g^t\left[\frac{1}{r}\frac{\partial (r v_r)}{\partial r} + \frac{\partial v_z}{\partial z} + \frac{\partial v_r}{\partial z} + \frac{1}{r}\frac{\partial (r v_z)}{\partial r}\right]\right]\left(\frac{1}{r}\frac{\partial (r v_r)}{\partial r} + \frac{\partial v_z}{\partial z}\right) - \varepsilon_g \rho_g \varepsilon - 2\beta k \quad (23)$$

D. Turbulence dissipation energy (in both phases):

$$\frac{\partial}{\partial r}(\varepsilon_g \rho_g \varepsilon v_r) + \frac{\partial}{\partial z}(\varepsilon_g \rho_g \varepsilon v_z) = \frac{1}{r}\frac{\partial}{\partial r}\left[r\varepsilon_g\left(\frac{\mu_g + \mu_g^t}{\sigma_\varepsilon}\right)\frac{\partial \varepsilon}{\partial r}\right] + \frac{\partial^2}{\partial z^2}\left[\varepsilon_g\left(\frac{\mu_g + \mu_g^t}{\sigma_\varepsilon}\right)\varepsilon\right] + C_{1\varepsilon}\frac{\varepsilon}{k}\left[\varepsilon_g \mu_g^t\left[\frac{1}{r}\frac{\partial (r v_r)}{\partial r} + \frac{\partial v_z}{\partial z} + \frac{\partial v_r}{\partial z} + \frac{1}{r}\frac{\partial (r v_z)}{\partial r}\right]\right]\left(\frac{1}{r}\frac{\partial (r v_r)}{\partial r} + \frac{\partial v_z}{\partial z}\right) - C_{2\varepsilon}\varepsilon_g \rho_g \frac{\varepsilon^2}{k} - 2\beta k \quad (24)$$

E. Kinetic reaction model:

A 14-lump model as developed by Lan *et al.*, [12] with its specific reaction paths and kinetic parameters is used in this analysis. The reaction scheme is shown in Figure 3. The reaction rate r_j of pseudo species j, in the component continuity equations (2-15) is expressed as:

$$r_j = -A_\alpha \cdot \frac{\emptyset(C_c)}{1 + K_h C_{ah}} \cdot \frac{\rho_g \rho_{ss}}{\varepsilon_g} K_i Y_i \quad (25)$$

where A_α is the correction coefficient of the initial catalyst activity, K_h is the adsorption coefficient of aromatics, $\emptyset(C_c)$ is the decay function of the catalyst due to coke depositing on the catalyst surface, calculated by:

$$\emptyset(C_c) = (1 + 0.51\, C_c)^{-2.75} \quad (26)$$

and the component concentration is

$$\rho_g C_i = Y_i\left(\frac{P}{RT}\right) \quad (27)$$

The heat of cracking reactions in W/m^3:

$$Q_r = -9.127X10^2 \frac{kJ}{kg\,coke} * mass\ of\ coke\ produced \quad (28)$$

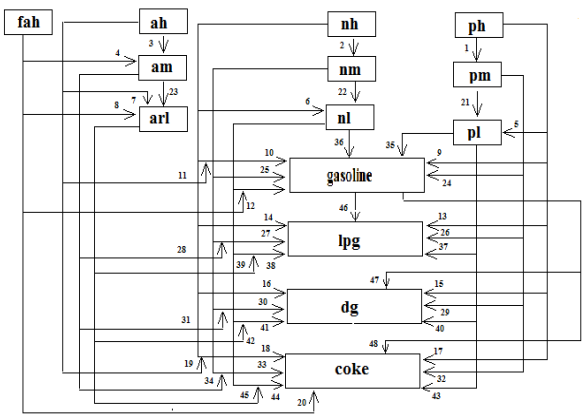

Figure 3. Reaction scheme of the 14-lumps RFCC kinetic model

F. Boundary Conditions

The implementation of correct inlet and boundary conditions is critical for a successful simulation of flow hydrodynamics and reaction behavior. The inlet component concentration in the bulk of the gas phase is taken from the feed composition, Y_i. While the inlet concentration inside the solid phase is based on the assumption that the regenerated catalyst pores are filled with steam only. Also with delta coke = 1.1515, the weight percent of carbon on regenerated catalyst = 0.011 and the inlet catalyst circulation rate = 1670 ton/hr [20,21]. Other inlet and operating conditions are in Table I.

Inlet conditions for gas phase

At the riser inlet, the air is supposed to enter the pipe with a parabolic axial velocity profile [11]:

$$v_{z,in}(r) = 2\frac{U_g}{(1-\varepsilon_{g,in})}\left[1-\left(\frac{r}{R}\right)^2\right] \quad (29)$$

where U_g is the superficial gas velocity.

Turbulent energy: $k_{in}(r) = 0.004 v_{z,in}^2(r)$ (30)

Dissipation rate of turbulent energy:

$$\varepsilon_{in} = \frac{2k_{in}^{3/2}\rho}{kd} \quad (31)$$

where k=0.4187, d is the inside diameter of the pipe.

Inlet conditions of particle phase

All variables were taken as having uniform distributions along radius [11]:

$$V_{gz,in} = \frac{U_g}{\varepsilon_{g,in}\rho_{sp}} \quad (32)$$

$$V_{gr,in} = 0 \quad (33)$$

$$k_{g,in} = 0.004 V_{gz,in}^2 \quad (34)$$

$$\varepsilon_{g,in} = \frac{2k_{g,in}^{3/2}}{kd} \quad (35)$$

TABLE I

OPERATING CONDITIONS AND PLANT DATA OF RFCC UNIT

Operating conditions:	
Reaction temperature (°C)	508
Reaction pressure (kPa)	361.3
Feed temperature (°C)	205.1
Catalyst inlet temperature (°C)	701
Average solid flux, kg/m^2.s	598
Feed flow rate (t/hr)	219.17
Process variables:	
Conversion	73.79
Catalyst to oil ratio, COR,	6.88
Catalyst circulation rate, (t/hr)	1670
Catalyst density, (kg/m^3)	1700
Recycle oil, (%vol of feed)	25
Catalyst property:	
Bulk density, kg/lit	0.65-0.75
Specific surface area, m^2/g	204
Particle size distribution, %wt :	
0 – 40 µm	19.4
40 – 70 µm	35.1
70 – 90 µm	16.7
> 90 µm	28.8
Product's yield, %wt:	
Dry gas	4.0
LPG	14.1
Gasoline	49.6
Diesel	23.0
Slurry	1.2
Coke	7.6
Loss	0.5
Total	100
Riser dimensions:	
Inside diameter, (m)	1.36
Height, (m)	47.1

$$\theta_{in} = 0.004 V_{gz,in}^2 \quad (36)$$

Outlet conditions for both phases

The fully developed condition of pipe flow is adopted [11]:

$$\frac{\partial \varphi}{\partial z} = 0 \quad where\ \varphi = v_g, v_s, k_g, \varepsilon_g, V_{gz}, V_{gr}, k_p, \varepsilon_p, \theta \quad (37)$$

Symmetric face: At symmetric face, $r = 0$

$$v_r = V_{gr} = 0, \quad \frac{\partial \varphi}{\partial z} = 0, \quad where\ \varphi = v_g, k_g, \varepsilon_g, V_{gz}, k_p, \varepsilon_p, \theta \quad (38)$$

Wall: At wall, $r = R$

$$v_z = v_r = V_{gz} = V_{gr} = 0, \quad k = k_p = 0, \quad \frac{\partial \varepsilon_g}{\partial r} = \frac{\partial \varepsilon_p}{\partial r} = 0 \quad (39)$$

III. NUMERICAL ASPECTS AND GRID INDEPENDENCE

The riser was simulated in 2D axi-symmetric steady state model. The finite-rate / eddy-dissipation in the turbulence - chemistry interaction was chosen to identify the rate of the 48 stoichiometric reactions. The governing equations are solved using the Phase Coupled SIMPLE (PCSIMPLE) algorithm for the pressure-velocity coupling and correction. The second order upwind discretization schemes were used to solve the convection terms.

Riser simulation with different mesh sizes was performed, and it is obvious that medium mesh size is sufficient for providing reasonable results. In general, the continuous increase in mesh density leads to slightly better results that are more grid-independent. However, the computational power currently available is still restricted significantly when using a finer mesh. Therefore, the mesh size used in simulating the riser is 75 × 400 grids (radial × axial).

IV. RESULTS AND DISCUSSION

The turbulent flow model of this work was validated with the experimental data of Bader *et al*., [22] and Lan *et al*., [12]. Table 2 shows the operating conditions and riser dimensions for both the above works. The model shows a good agreement with Bader *et al*., [22] experimental data and the model results of Lan *et al*., [12] in the solid phase volume fraction comparison, as illustrated in Figures 4 and 5. However, in Figure 5, it gives higher axial velocity for the particles near the wall.

TABLE 2

OPERATING CONDITIONS USED FOR COMPARISON

Operating conditions	Bader et al.	Lan et al.	
		1st stage riser	2nd stage riser
Catalyst type	FCC	Zeolite	Zeolite
Particle diameter (µm)	76	76	76
Particle density (Kg/m^3)	1714	1714	1714
Particle mass flux(Kg/m^2 s)	98	300	90
Superficial gas velocity, m/s	3.7	3.7	3.7
Reaction temperature, °C		500	506
COR		5.46	6.07
Inlet pressure, kPa		299.55	304.7
Pre-lift steam, kg/s		0.12	0.056

Also Sundaresan [23] in his plenary session paper at the international conference of CFB-10 states that the volume fraction of particles in the riser is generally small enough that the particles interact with each other primarily through collisions, while in standpipes (downers) it is usually high enough that stress transmission can occur through collisions as well as sustained frictional contact between the particles and between the particles and the wall. Risers typically operate in the so-called fast-fluidization regime where there is a denser bottom region, transitioning to a more dilute flow at the top. Furthermore, the time-averaged particle volume

fraction and gas and particle mass fluxes manifest significant lateral variations; particle volume fractions generally tend to be high near the riser walls where the mass flux of particles is frequently negative (i.e. down flow) even though the cross-sectional averaged mass flux of particles is positive. The particles tend to drag the gas downward in the wall region, and so there can be significant internal recirculation of both particles and gas in the riser. At very high gas velocities, the down flow disappears and one can even get a higher mass flux of particles at the wall region than the core [23]. Therefore, when changing the drag model for the momentum phase interaction from Gidaspaw [13] (which was used by Lan *et al*., [12] also) to Matsen drag model (that was modified by Vaishali *et al*., [17]), the particle velocity profile get maximum value at the wall region and minimum value at the centre. Figure 6 shows the particle velocity profile, and Figure 7 shows the contour of this velocity along the riser.

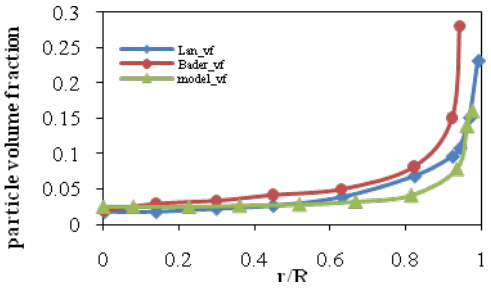

Figure 4. Comparison of particle volume fraction

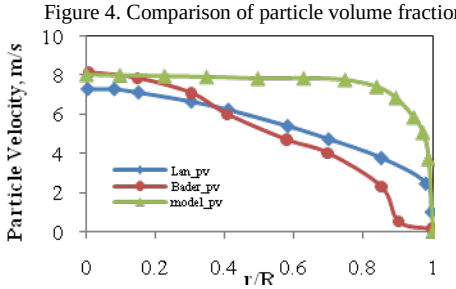

Figure 5. Comparison of axial solid velocity

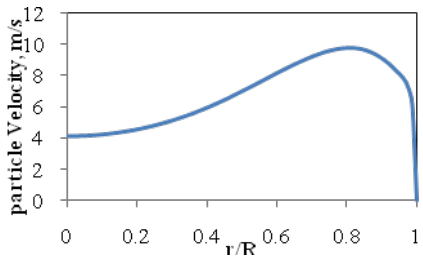

Figure 6. Axial solid velocity when modeling with ***Matsen*** drag coefficient

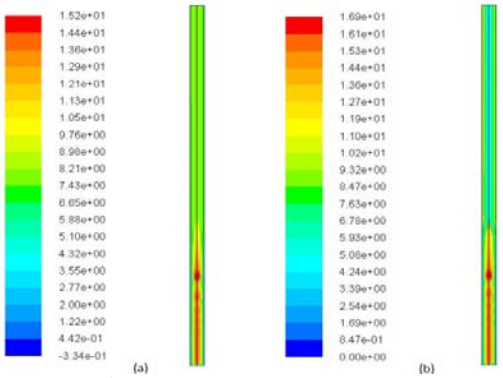

Figure 7. Contours of the axial solid velocity: (a) with Gidaspaw drag model, (b) with Matsen drag model

One of the factors that affects the products yields and reaction rate is reaction temperature, that should be kept between 480-520 ^{o}C. Another factor that affect the reaction rate is the catalyst activity, which decreases sharply in the riser entry zone, and then slowly in the later half of the riser. This distribution of catalyst activity has a significant influence on the cracking reactions and product distribution in the riser. Figures 8, 9, and 10 show how the heavy oil components concentration decrease sharply in the first 10 meters, producing the beak values for the mass fraction of medium and light oils. Then the medium and light oils concentration decrease sharply due to overcracking in the next 10 meters producing gasoline, gases and coke. This means that the oil cracking is an instantaneous reaction. The predicted yield of light gases (lpg, dry gas) and coke is higher on the case of residual feedstock, as shown in Figure 11. Great consistency between these predicted profiles and the results of Lan *et al*., [12]. Also it is in a very good agreement with the product yield data obtained from the industrial plant data in Table1. The main goal of this RFCC unit is to maximize gasoline production, this explain the higher gasoline yield in Figure 12. It is higher than the yield from plant data and from Lan *et al*., [12]. Optimum value for gasoline yield can be found by adjusting many parameters like process variables and kinetic parameters in the next future work.

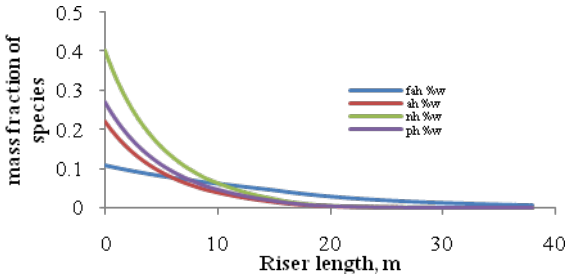

Figure 8. Heavy components mass fraction profiles along the riser

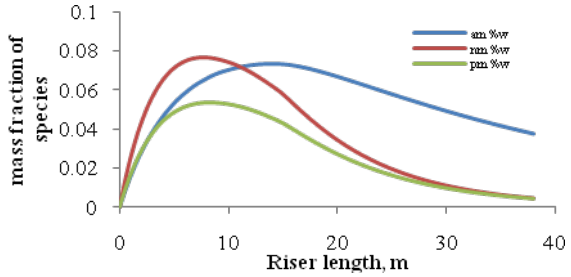

Figure 9. Medium components mass fraction profiles along the riser

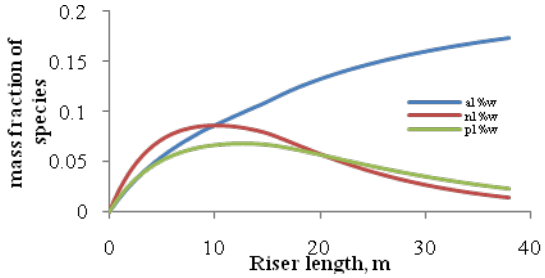

Figure 10. Light components mass fraction profiles along the riser

Catalyst flux and volume fraction has a great effect on the yield of cracking products since catalytic cracking reactions must occur over the catalyst surface. This explains the increases in the radial mass fraction profiles of the products. Figure 13 and 14 illustrate the radial distribution of gasoline,

gases and coke in the riser at two levels, at the outlet (38m) and in the middle of the riser (19m).

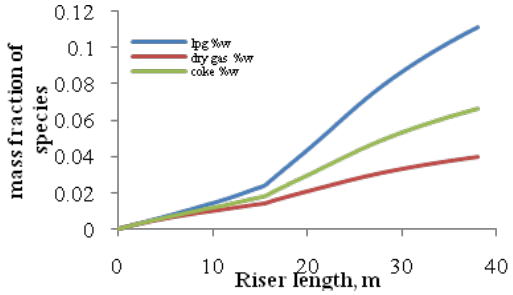

Figure 11. Light gases and coke mass fraction profiles along the riser

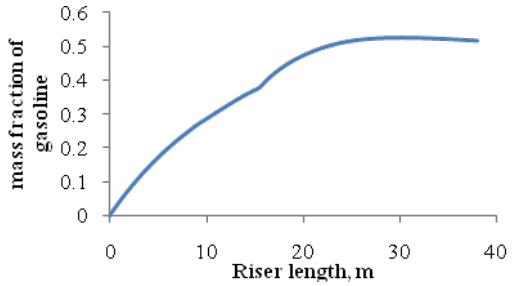

Figure 12. Gasoline mass fraction profiles along the riser

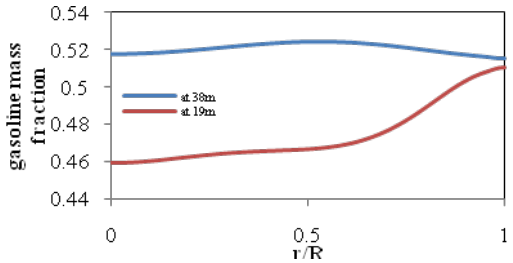

Figure 13. Radial variation of gasoline mass fraction at the out let level and middle of the riser height

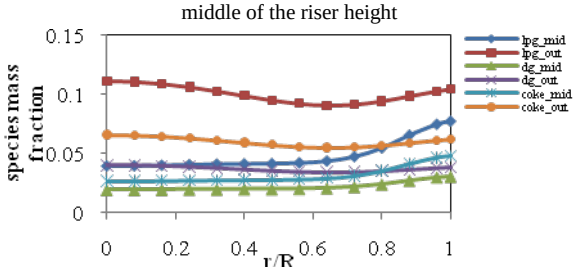

Figure 14. Radial variation of gases and coke mass fractions at the out let level and middle of the riser height

V. CONCLUSIONS

In commercial applications of RFCC unit, an optimization process is very important for the design aspects or during operations. Therefore, the CFD approach was applied to simulate the flow behavior and catalytic cracking reactions in RFCC riser reactor. The standard k-ε per phase model for the turbulent flow, and the 14-lump kinetic model of the cracking reactions were used together with the drag models to simulate the riser in ANSYS FLUENT 13.0. The results show sufficient agreement with the plant data and other works data. Thus the model can be validly used for an optimization.

ACKNOWLEDGMENT

Authors are grateful to Universiti Technologi Pertonas (UTP) for providing all the support to undertake this research work. Also they would like to acknowledge Ms Mary and Mr. Lei from Woshan Tecknology Co. Ltd, China.

REFERENCES

[1] R. A. Meyers, D. A. Hunt, "Handbook of Petroleum Refining Processes," McGraw-Hill, 2003.

[2] K. N. Theologos, A. I. Lygeros, N. C. Markatos, "Feedstock Atomization Effects on FCC Riser Reactions Selectivity," *Chem. Eng. Sci*. 1999, 54, 5617.

[3] T. A. Berry, T. R. McKeen, T. S. Pugsley, and A. K. Dalai, "Two-Dimensional Reaction Engineering Model of the Riser Section of a Fluid Catalytic Cracking Unit," *Ind. Eng. Chem. Res*., 2004, 43 (18), pp.5571-5581• DOI: 10.1021/ie0306877 • Publication Date (Web): 21 April 2004

[4] A. Gupta, D. Subbarao, "Model for the performance of fluid catalytic cracking (FCC) riser reactor: Effect of feed atomization," *Chemical Engineering Science*, 56(2001), 4489–4503.

[5] A. Gupta, D. Subbarao, "Effect of feed atomization on FCC performance: simulation of entire unit," *Chemical Engineering Science*, 58(2003), pp. 4567–4579.

[6] J. A. Souzaa, J. V. C. Vargasa, O. F. Von Meiena, and W. Martignonib**,** "Numerical simulation of FCC risers," *Engenharia Térmica*, n‡ 4, 2003, pp. 17-21.

[7] R. K. Gupta, V. Kumara, V.K. Srivastavab, "Anew generic approach for the modeling of fluid catalytic cracking (FCC) riser reactor," *Chemical Engineering Science* 62 , 2007, pp. 4510 – 4528

[8] A. K. Das, E. Baudrez, G. B. Marin, and G. J. Heynderickx, "Three-Dimensional Simulation of a Fluid Catalytic Cracking Riser Reactor," *Ind. Eng. Chem. Res.*, 2003, 42 (12), 2602-2617• DOI: 10.1021/ie020744g • Publication Date (Web): 22 April 2003

[9] F. Hernandez-Jimeneza, J.R. Thirdb, A. Acosta-Iborraa, C.R. Mullerb " Critical evaluation of Euler-Euler AND Euler-Lagranian modeling strategies in a 2-D gas fluidized bed," conference paper : CFB 10, May 1st through 5th, 2011, Sunriver, Oregon, USA, section 11-2

[10] K.N. Theologos, N.C. Markatos, "Advanced modeling of fluid catalytic cracking riser-type reactors," *A.I.Ch.E. Journal* 39, 1993, pp. 1007–1017.

[11] Y. Zheng, X. Wan, Z. Qian, F. Wei, Y. Jin, " Numerical simulation of the gas-particle turbulent flow in riser reactor based on k-ε-k_p-ε_p-Θ two-fluid model," *Chemical Engineering Science*, 56, 2001, pp. 6813 – 6822

[12] X. Lan, C. Xu, G. Wang, L. Wu, J. Gao, "CFD modeling of gas-solid flow and cracking reaction in two-stage riser FCC reactors," *Chemical Engineering Science* 64 (2009) 3847 – 3858

[13] D. Gidaspow, "Multiphase Flow and Fluidization: Continuum and Kinetic Theory Description," *Academic Press, New York*, 1994.

[14] H. Arastoopour, P. Pakdel, M. Adewumi, "Hydrodynamic analysis of dilute gas–solids flow in a vertical pipe," *Powder Technol*. 62, 1990, pp. 163–170.

[15] M. Syamlal, T. O, Brien, "Derivation of a drag coefficient from velocity–voidage correlation," U.S. Dept. of Energy, Office of Fossil Energy, National Energy Technology Laboratory, Morgantown, West Virginia, April, 1987.

[16] A. Almuttahar, F. Taghipour, "Computational fluid dynamics of high density circulating fluidized bed riser: Study of modeling parameters," *Powder Technology* 185, 2008, pp. 11–23

[17] S. Vaishali, S. Roy, P. L. Mills, "Hydrodynamic simulation of gas–solids downflow reactors," *Chemical Engineering Science*, 63, 2008, pp. 5107-5119

[18] Matsen, J.M., "Mechanisms of choking and entrainment," *Powder Technology*, 32, 1982, pp. 22–33.

[19] Peng Li, X. Lan, C. Xu, G. Wang, C. Lu, J. Gao, "Drag models for simulating gas–solid flow in the turbulent fluidization of FCC particles" *Particuology*, 7 , 2009, pp. 269–277

[20] R. M. Ansari and M. O. Tadé, "Constrained nonlinear multivariable control of a fluid catalytic cracking process," *Elsevier Science Ltd*., 2000.

[21] ENSPM Formation Industrie, "Refining-Petrochemicals-Chemicals-Engineering Data Book," 1999

[22] R. Bader, J. Findlay, T.M. Knowlton, "Gas/solids flow patterns in a 30.5cm diameter circulating fluidized bed," In: Basu, P., Large, J.F. (Eds.), *Circulating Fluidized Bed Technology 2*. Pergamon Press, Oxford, UK, 1988, pp. 123–137.

[23] International Conference on Circulating Fluidized Beds and Fluidization Technology , CFB 10, May 1st through 5th, 2011, Sunriver Resort, Sunriver, Oregon, USA.